Orbital degree of freedom and phase separation in ferromagnetic manganites at finite temperatures

S. Okamoto, S. Ishihara, and S. Maekawa
Institute for Materials Research, Tohoku University, Sendai, 980-8577 Japan
(Received 19 February 1999)

The spin and orbital phase diagram for perovskite manganites is investigated as a function of temperature and hole concentration. The superexchange and double exchange interactions dominate the ferromagnetic phases in the lightly and moderately doped regions of holes, respectively. The two interactions favor different orbital states. Between the phases, two interactions compete with each other and the phase separation appears in the wide range of temperature and hole concentration. The anisotropy of the orbital space causes discontinuous changes of the orbital state and promotes the phase separation.

I. INTRODUCTION

Doped perovskite manganites $A_{1-x}B_x\mathrm{MnO_3}$ (A: La, Pr, Sm, B: Sr, Ca) and their related compounds have attracted much attention, since they show not only the colossal magnetoresistance (CMR) (Refs. 1–4) but a lot of dramatic and wide variety of phenomena. Although the ferromagnetic phase commonly appears in the manganites, the origin still remains to be clarified. Almost a half-century ago, the double exchange (DE) interaction was proposed to explain the correlation between the appearance of ferromagnetism and the metallic conductivity below Curie temperature.[5,6] In the scenario, the Hund coupling between carriers and localized t_{2g} spins was stressed. The ferromagnetic metallic state in the moderately doped region is understood based on this interaction, where the compounds show the wide band width.[7,8]

On the contrary, the DE scenario is not applied to the lightly doped region[9] ($x<0.2$) where the CMR effect is observed. In the region, the degeneracy of e_g orbitals in a Mn^{3+} ion termed the orbital degree of freedom is one of the important ingredients. With taking into account the orbital degree together with electron correlation, the additional ferromagnetic interaction, that is, the ferromagnetic superexchange (SE) interaction, is derived. This is associated with the alternate alignment of the orbital termed antiferro(AF)-type orbital ordering.[10–12] The SE interaction brings about the ferromagnetic spin alignment in the ab plane in $\mathrm{LaMnO_3}$ and the quasi-two-dimensional dispersion relation of the spin wave in it.[13,14] When holes are introduced into $\mathrm{LaMnO_3}$, the magnetic and transport properties rapidly change as two-dimensional ferromagnetic (A-type AF) insulator → isotropic ferromagnetic insulator → ferromagnetic metal.[3,15] In the intermediate doping region, the first order phase transition between the ferromagnetic metallic state to the ferromagnetic insulating one has been recently discovered in $\mathrm{La_{1-x}Sr_xMnO_3}$ with $x\sim0.12$.[16] In the ferromagnetic insulating phase at low temperature, the orbital ordering is directly observed by the resonant x-ray scattering where the cooperative Jahn-Teller distortion is significantly diminished; the ferromagnetic interaction does not originate from the Jahn-Teller distortion but the superexchange process under the correlation of electrons. This result suggests that the two ferromagnetic interactions contend with each other and the orbital degree of freedom controls the domination between the two. In order to understand a dramatic change of electronic states in this doping region and its relation to CMR, it is indispensable to study the mutual relation between the two ferromagnetic interactions, i.e., DE and SE.

In this paper, we investigate the spin and orbital phase diagram as a function of temperature (T) and hole concentration (x). We focus on the competition and cooperation between the two ferromagnetic interactions SE and DE. We show that the SE and DE interactions dominate the ferromagnetic phases in the lightly and moderately doped regions of holes, respectively, and favor the different orbital structures of each other. Between the two phases, the phase separation (PS) appears in the wide range of x and T. It is shown that PS is promoted by the anisotropy in the orbital space. The spin and orbital phase diagram at $T=0$ was obtained by the Hartree-Fock theory and interpreted in terms of the SE and DE interactions in Ref. 17. The PS state between two ferromagnetic phases driven by the DE interaction and the Jahn-Teller distortion at $T=0$ was discussed in Ref. 18. In this paper, we obtain the PS state based on the model with strong correlation of electrons at finite T.

In Sec. II, the model Hamiltonian, where the electron correlation and the orbital degeneracy are taken into account, is introduced. In Sec. III, formulation to calculate the phase diagram at finite T and x is presented. Numerical results are shown in Sec. IV and the last section is devoted to summary and discussion.

II. MODEL

Let us consider the model Hamiltonian which describes the electronic structure in perovskite manganites. We set up the cubic lattice consisting of manganeses ions. Two e_g orbitals are introduced in each ion and t_{2g} electrons are treated as a localized spin ($\vec{S}_{t_{2g}}$) with $S=3/2$. Between e_g electrons, three kinds of the Coulomb interaction, that is, the intraorbital Coulomb interaction (U), the interorbital one (U'), and the exchange interaction (I), are taken into account. There also exist the Hund coupling (J_H) between e_g and t_{2g} spins and the electron transfer $t_{ij}^{\gamma\gamma'}$ between site i with orbital γ

and site j with γ'. Among these energies, the Coulomb interactions are the largest one. Therefore, by excluding the doubly occupied state at each site, we derive the effective Hamiltonian describing the low energy spin and orbital states:[14]

$$\mathcal{H}=\mathcal{H}_t+\mathcal{H}_J+\mathcal{H}_H+\mathcal{H}_{AF}. \tag{1}$$

The first and second terms correspond to the so-called t and J terms in the tJ model for e_g electrons, respectively. These are given by

$$\mathcal{H}_t=\sum_{\langle ij\rangle\gamma\gamma'\sigma} t_{ij}^{\gamma\gamma'}\tilde{d}_{i\gamma\sigma}^{\dagger}\tilde{d}_{j\gamma'\sigma}+\text{H.c.} \tag{2}$$

and

$$\mathcal{H}_J=-2J_1\sum_{\langle ij\rangle}\left(\frac{3}{4}n_in_j+\vec{S}_i\cdot\vec{S}_j\right)\left(\frac{1}{4}-\tau_i^l\tau_j^l\right)$$
$$-2J_2\sum_{\langle ij\rangle}\left(\frac{1}{4}n_in_j-\vec{S}_i\cdot\vec{S}_j\right)\left(\frac{3}{4}+\tau_i^l\tau_j^l+\tau_i^l+\tau_j^l\right), \tag{3}$$

where

$$\tau_i^l=\cos\left(\frac{2\pi}{3}n_l\right)T_{iz}-\sin\left(\frac{2\pi}{3}n_l\right)T_{ix}, \tag{4}$$

and $(n_x,n_y,n_z)=(1,2,3)$. l denotes the direction of bond connecting i and j sites. $\tilde{d}_{i\gamma\sigma}$ is the annihilation operator of e_g electron at site i with spin σ and orbital γ with excluding double occupancy. $\vec{S}_i$ is the spin operator of the e_g electron and $\vec{T}_i$ is the pseudospin operator for the orbital degree of freedom defined as $\vec{T}_i=(1/2)\Sigma_{\sigma\gamma\gamma'}\tilde{d}_{i\gamma\sigma}^{\dagger}(\vec{\sigma})_{\gamma\gamma'}\tilde{d}_{i\gamma'\sigma}$. $J_1=t_0^2/(U'-I)$ and $J_2=t_0^2/(U'+I+2J_H)$ where t_0 is the transfer intensity between $d_{3z^2-r^2}$ orbitals in the z direction, and the relation $U=U'+I$ is assumed. The orbital dependence of $t_{ij}^{\gamma\gamma'}$ is estimated from the Slater-Koster formulas. The third and fourth terms in Eq. (1) describe the Hund coupling between e_g and t_{2g} spins and the antiferromagnetic interaction between t_{2g} spins, respectively, as expressed as

$$\mathcal{H}_H=-J_H\sum_i \vec{S}_{t_{2g}i}\cdot\vec{S}_i \tag{5}$$

and

$$\mathcal{H}_{AF}=J_{AF}\sum_{\langle ij\rangle}\vec{S}_{t_{2g}i}\cdot\vec{S}_{t_{2g}j}. \tag{6}$$

The detailed derivation of the Hamiltonian is presented in Ref. 14. Main features of the Hamiltonian are summarized as follows. (1) This is applicable to doped manganites as well as undoped insulators. (2) Since $J_1>J_2$, the ferromagnetic state associated with the AF-type orbital order is stabilized by $\mathcal{H}_J$. Therefore, two kinds of the ferromagnetic interaction, that is, SE and DE are included in the model. (3) As seen in $\mathcal{H}_J$, the orbital pseudospin space is strongly anisotropic unlike the spin space. The lattice degree of freedom is neglected in the model, since the cooperative Jahn-Teller distortion is diminished around $0.1<x<0.2$ in $La_{1-x}Sr_xMnO_3$ and is not a relevant factor to investigate two kinds of the ferromagnetic interaction.[16] The inter site Coulomb interaction is not included in the model. Although the interaction may modify detail structures of the orbital ordered state and a shape and size of hole rich/poor regions in the phase separated states, the present model provides a proper starting point to describe the competition between the two ferromagnetic interactions of our present interest.

III. FORMULATION

In order to calculate the spin and orbital states at finite temperatures and investigate the phase separation, we generalize the mean field theory proposed by de Gennes.[19] From now on, the spin ($\vec{S}$) and pseudospin ($\vec{T}$) variables are denoted by $\vec{u}$ in the unified fashion. The spin and orbital pseudospin are treated as classical vectors as follows:

$$(S_{ix},S_{iy},S_{iz})=\frac{1}{2}(\sin\theta_i^s\cos\phi_i^s,\sin\theta_i^s\sin\phi_i^s,\cos\theta_i^s) \tag{7}$$

and

$$(T_{ix},T_{iy},T_{iz})=\frac{1}{2}(\sin\theta_i^t,0,\cos\theta_i^t), \tag{8}$$

where the motion of the pseudospin is assumed to be confined in the xz plane. θ_i^t in Eq. (8) characterizes the orbital state at site i as

$$|\theta_i^t\rangle=\cos(\theta_i^t/2)|d_{3z^2-r^2}\rangle+\sin(\theta_i^t/2)|d_{x^2-y^2}\rangle. \tag{9}$$

t_{2g} spins are assumed to be parallel to the e_g one. The thermal distributions of spin and pseudospin are described by the distribution function which is a function of the relative angle between $\vec{u}_i$ and the mean field $\vec{\lambda}_i^u$,

$$w_i^u(\vec{u}_i)=\frac{1}{\nu^u}\exp\left(\vec{\lambda}_i^u\cdot\frac{\vec{u}_i}{|\vec{u}_i|}\right), \tag{10}$$

where the normalization factor is defined by

$$\nu^s=\int_0^{\pi}d\theta^s\int_0^{2\pi}d\phi\sin\theta^s\exp(\lambda^s\cos\theta^s) \tag{11}$$

and

$$\nu^t=\int_0^{2\pi}d\theta^t\exp(\lambda^t\cos\theta^t). \tag{12}$$

By utilizing the distribution functions defined in Eq. (10), the expectation values of operators $A_i(\vec{S}_i)$ and $B_i(\vec{T}_i)$ are obtained as

$$\langle A_i\rangle_s=\int_0^{\pi}d\theta^s\int_0^{2\pi}d\phi^s\sin\theta^s w_i^s(\vec{S}_i)A_i(\vec{S}_i) \tag{13}$$

and

$$\langle B_i\rangle_t=\int_0^{2\pi}d\theta^t\,w_i^t(\vec{T}_i)B_i(\vec{T}_i), \tag{14}$$

respectively. In this scheme, the free energy is represented by summation of the expectation values of the Hamiltonian and the entropy of spin and pseudospin as follows:

$$\mathcal{F}=\langle\mathcal{H}\rangle_{s,t}-NT(\mathcal{S}^s+\mathcal{S}^t). \tag{15}$$

N is the number of Mn ions and $\mathcal{S}^u$ is the entropy calculated by

$$\mathcal{S}^u=-\langle \ln w^u(\vec{u})\rangle_u . \tag{16}$$

It is briefly noticed that the above formulation gives the unphysical states at very low temperatures ($T<T_{\rm neg}\sim J_{1(2)}/10$) where the entropy becomes negative. This is because the spin and pseudospin are treated as the classical moments. Therefore, we restrict our calculation in the region above $T_{\rm neg}$ and $T=0$ where the full polarizations of spin and pseudospin are assumed. Since the spin (pseudospin) moment is almost saturated far above $T_{\rm neg}$ in the wide range of x, an extrapolation of the result calculated above $T_{\rm neg}$ smoothly connects to that at $T=0$.

Next, we concentrate on the calculation of $\langle\mathcal{H}\rangle_{s,t}$ in Eq. (15). As mentioned later, two kinds of sublattice termed A and B are introduced for both the spin and orbital orderings. The spin (pseudospin) operator and the mean field in $A(B)$ sublattice are represented by $\vec{S}_{A(B)}$ ($\vec{T}_{A(B)}$) and $\vec{\lambda}^s_{A(B)}$ ($\vec{\lambda}^t_{A(B)}$), respectively, with the condition of $|\vec{\lambda}^{s(t)}_A|=|\vec{\lambda}^{s(t)}_B|\equiv\lambda^{s(t)}$. The spin part $\vec{S}_i\cdot\vec{S}_j$ in $\mathcal{H}_J$ is rewritten as $m^{s2}\cos\Theta^s$ where $m^s(=\langle\vec{S}_A\cdot\vec{\lambda}^s_A/\lambda^s\rangle_s)$ is the magnetization of spin and Θ^s is the relative angle between $\vec{\lambda}^s_A$ and $\vec{\lambda}^s_B$. On the other hand, the orbital part in $\mathcal{H}_J$ includes the terms $m^{t2}\cos(\Theta^t_A+\Theta^t_B)$ and $m^{t2}\cos(\Theta^t_A-\Theta^t_B)$, where $m^t(=\langle\vec{T}_A\cdot\vec{\lambda}^t_A/\lambda^t\rangle_t)$ is the magnetization of pseudospin and $\Theta^t_{A(B)}$ is the absolute angle of $\vec{\lambda}^t_{A(B)}$ in the pseudospin space. The definition of $\Theta^t_{A(B)}$ is the same as that of θ^t_i in Eqs. (8) and (9). This is because of the anisotropy in the orbital space. $\mathcal{H}_{AF}$ is also rewritten by m^s and Θ^s under the relation of $\langle\vec{S}\rangle_s=4\langle\vec{S}_{t_{2g}}\rangle_s$. As for the transfer term $\mathcal{H}_t$, we introduce the rotating frame[20] and decompose the electron operator as $\tilde{d}_{i\gamma\sigma}=h^\dagger_i z^s_{i\sigma}z^t_{i\gamma}$, where $h^\dagger_i$ is a spinless and orbital-less fermion operator and $z^s_{i\sigma}$ and $z^t_{i\gamma}$ are the elements of the unitary matrix U^u in the spin and pseudospin frames, respectively. U^u is defined by

$$U^u=\begin{pmatrix} z^u_{i\uparrow} & -z^{u*}_{i\downarrow}\\ z^u_{i\downarrow} & z^{u*}_{i\uparrow}\end{pmatrix}, \tag{17}$$

with $z^s_{i\uparrow}=\cos(\theta^s_i/2)e^{-i\phi^s_i/2}$ and $z^s_{i\downarrow}=\sin(\theta^s_i/2)e^{i\phi^s_i/2}$ for spin, and $z^t_{i\uparrow}=\cos(\theta^t_i/2)$ and $z^t_{i\downarrow}=\sin(\theta^t_i/2)$ for orbital. By using the form, $\mathcal{H}_t$ is rewritten as

$$\mathcal{H}_t=\sum_{\langle ij\rangle} t^s_{ij}t^t_{ij}h_ih^\dagger_j+\text{H.c.}, \tag{18}$$

with $t^s_{ij}=\Sigma_\sigma z^{s*}_{i\sigma}z^s_{j\sigma}$ and $t^t_{ij}=\Sigma_{\gamma\gamma'}z^{t*}_{i\gamma}t^{\gamma\gamma'}_{ij}z^t_{j\gamma'}$. The former gives $e^{i(\phi^s_i-\phi^s_j)/2}\cos\theta^s_i\cos\theta^s_j-e^{-i(\phi^s_i-\phi^s_j)/2}\sin\theta^s_i\sin\theta^s_j$ as expected from the double exchange interaction.[6] It is known that this kind of decomposition of the electron operator and the mean field approximation are suitable to describe the ordered state of the present interest. By diagonalizing the energy in the momentum space, $\mathcal{H}_t$ is given by

$$\mathcal{H}_t=\sum_{\vec{k}}\sum_{l=1}^{N_l}\varepsilon^l_{\vec{k}}h^\dagger_{l\vec{k}}h_{l\vec{k}}, \tag{19}$$

where l indicates the band of $h_{l\vec{k}}$ and N_l is the number of the bands. $\varepsilon^l_{\vec{k}}$ corresponds to the energy of the lth band. Thus, the expectation value of $\mathcal{H}_t$ per site is obtained by

$$E_t=\left\langle\frac{1}{N}\sum_{\vec{k}}\sum_{l=1}^{N_l}\varepsilon^l_{\vec{k}}f_F(\varepsilon^l_{\vec{k}}-\varepsilon_F)\right\rangle_{s,t}. \tag{20}$$

ε_F in Eq. (20) is the Fermi energy of $h_{i\vec{k}}$ determined in the equation

$$x=\frac{1}{N}\sum_{\vec{k}}\sum_{l=1}^{N_l}f_F(\varepsilon^l_{\vec{k}}-\varepsilon_F), \tag{21}$$

where $f_F(\varepsilon)$ is the Fermi distribution function. As a result, $\langle\mathcal{H}\rangle_{s,t}$ is represented as a function of Θ^s, $\Theta^t_{A(B)}$, and $\lambda^{s(t)}$. By minimizing $\mathcal{F}$ with respect to them, the mean field solutions are obtained. We confirm that the global feature of the calculated phase diagram at $T=0$ without the PS state is consistent with ones obtained by the Hartree-Fock theory and the auxiliary boson approach.[17,21]

IV. NUMERICAL RESULTS

A. Phase diagram at $T=0$

In this subsection, we show the numerical results at $T=0$. For examining both spin and orbital orderings, two kinds of sublattice are introduced. We assume ferromagnetic (F)-type and three kinds of antiferromagnetic (AF)-type spin (orbital) orderings, which are layer (A) type, rod (C) type, and NaCl (G) type. A type of the orbital in the AF-type orbital ordering is represented by $(\Theta^{(t)}_A/\Theta^{(t)}_B)$.

In Fig. 1(a), the ground state energy ($E_{\rm GS}$) is shown as a function of hole concentration (x) for several values of $J_{\rm AF}/t_0$. Double- or multiple-minima appear in the $E_{\rm GS}$-x curve depending on the value of $J_{\rm AF}/t_0$. Therefore, the homogenous phase is not stable against the phase separation. This feature is remarkable in the region of $0.1<x<0.4$. In Fig. 1(b), $E_{\rm GS}$ is decomposed into $\langle\mathcal{H}_t\rangle$ and $\langle\mathcal{H}_J\rangle$ for $J_{\rm AF}/t_0=0$. By drawing a tangent line in the $E_{\rm GS}$-x curve as shown in Fig. 1(a), the phase separation is obtained. By using the so-called Maxwell construction, the phase diagram at $T=0$ is obtained in the plane of $J_{\rm AF}$ and x (Fig. 2). The parameter values are chosen to be $J_1/t_0=0.25$ and $J_2/t_0=0.0625$. $J_{\rm AF}/t_0$ for manganites is estimated from the Néel temperature in $CaMnO_3$ to be $0.001\sim0.01$. Let us consider the case of $J_{\rm AF}/t_0=0.004$. With doping of holes, the magnetic structure is changed as A-AF$\rightarrow$PS(A-AF/F_1)$\rightarrow F_1\rightarrow$PS($F_1/F_2$)$\rightarrow F_2$, where PS($A/B$) implies the phase separation between A and B phases. The canted spin structure does not appear. F_1 and F_2 are the two kinds of ferromagnetic phase discussed below in more detail. Between F_1 and F_2 phases, the PS state appears and dominates the large region of the phase diagram. For example, at $x=0.2$, the F_1 and F_2 phases coexist with the different volume fractions of

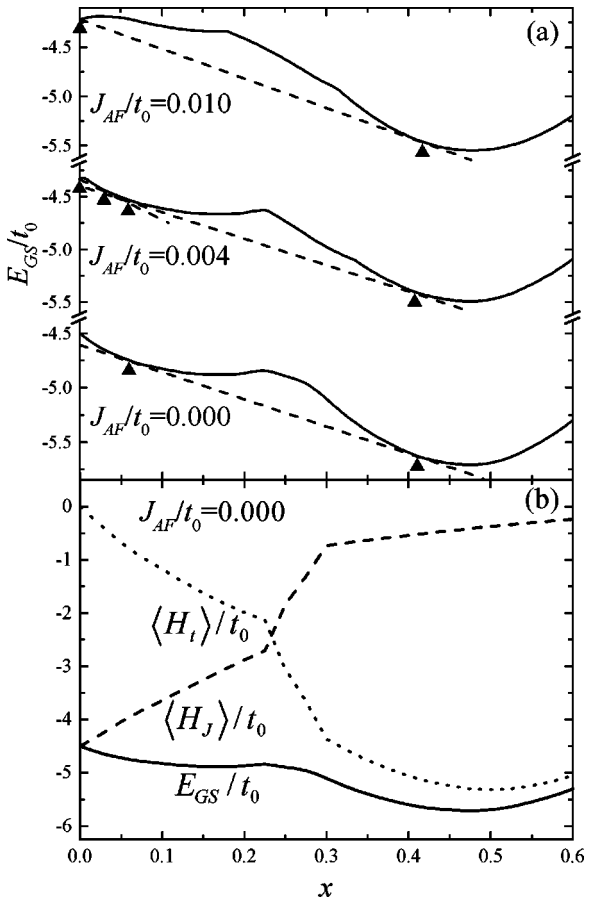

FIG. 1. The ground state energy ($E_{\rm GS}$) as a function of hole concentration (x). (a): $J_{\rm AF}/t_0$ is chosen to be 0, 0.004, and 0.01. The broken lines and the filled triangles show the tangent lines of the E_{GS}-x curve and the points of contact between the two, respectively. (b): $E_{\rm GS}$ is decomposed into the contributions from $\langle \mathcal{H}_t \rangle$ and $\langle \mathcal{H}_J \rangle$. $J_{\rm AF}/t_0$ is chosen to be 0. The other parameter values are $J_1/t_0=0.25$, and $J_2/t_0=0.0625$.

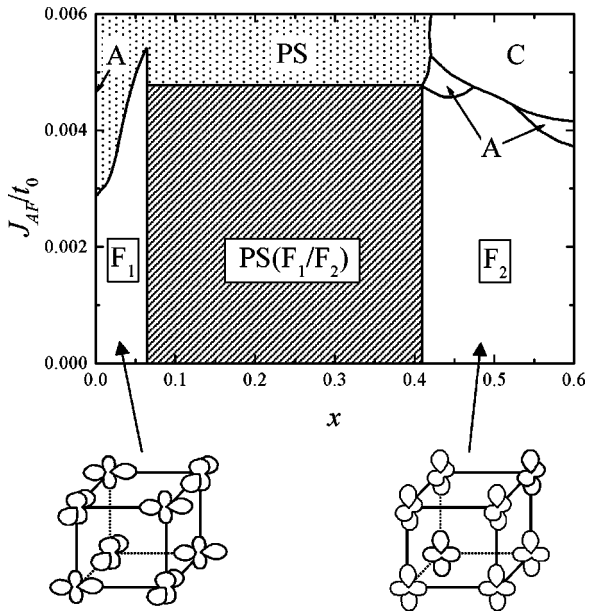

FIG. 2. The phase diagram at $T=0$ in the plane of antiferromagnetic interaction $J_{\rm AF}$ and hole concentration x. F_1 and F_2 are the ferromagnetic phases with different types of orbital ordering. PS(F_1/F_2) is the phase separated state between the F_1 and F_2 phases. Types of orbital ordering in the two phases are schematically presented. In the dotted region, there exist PS(A-AF/F_1) and PS(A-AF/C-AF). The parameter values are chosen to be $J_1/t_0=0.25$ and $J_2/t_0=0.0625$.

60 and 40 %, respectively. We also find the PS state between A-AF and F_1 phases in the region of $0.0<x<0.03$.

Now we focus on two kinds of ferromagnetic phase and the PS state between them. The F_1 and F_2 phases originate from the SE interaction between e_g orbitals and the DE one, respectively. The interactions have different types of orbital ordering as shown in Fig. 2. These are the C type[22] with $(\Theta_A^t/\Theta_B^t)=(\pi/2,3\pi/2)$ and the A type with $(\Theta_A^t/\Theta_B^t)=(\pi/6,-\pi/6)$, respectively. It is known that the AF-type orbital ordering obtained in the F_1 phase is favorable to the ferromagnetic SE interaction through the coupling between spin and orbital degrees in $\mathcal{H}_J$. On the other hand, the F-type orbital ordering promotes the DE interaction by increasing the gain of the kinetic energy. To show the relation between the orbital ordering and the kinetic energy, we present the density of state (DOS) of the spinless and orbital-less fermions in the F_1 and F_2 phases in Figs. 3(a) and 3(b), respectively. It is clearly shown that the band width in the F_2 phase is larger than that in the F_1 phase. In addition, DOS in the F_2 phase has a broad peak around $-2<\omega/t_0<-0.8$ which results from the quasi-one-dimensional orbital ordering. Because of the structure in DOS, the kinetic energy further decreases in the F_2 phase more than the F_1 phase.

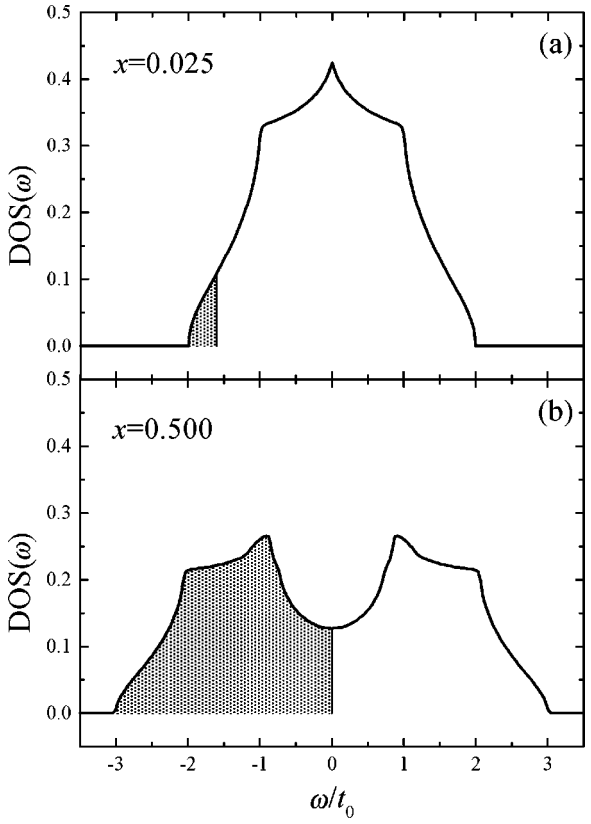

FIG. 3. The densities of state (DOS) for the spinless and orbital-less fermions $h_{\vec{k}}$ (a) in the F_1 phase and (b) in the F_2 phase. The shaded areas show the occupied state of $h_{\vec{k}}$.

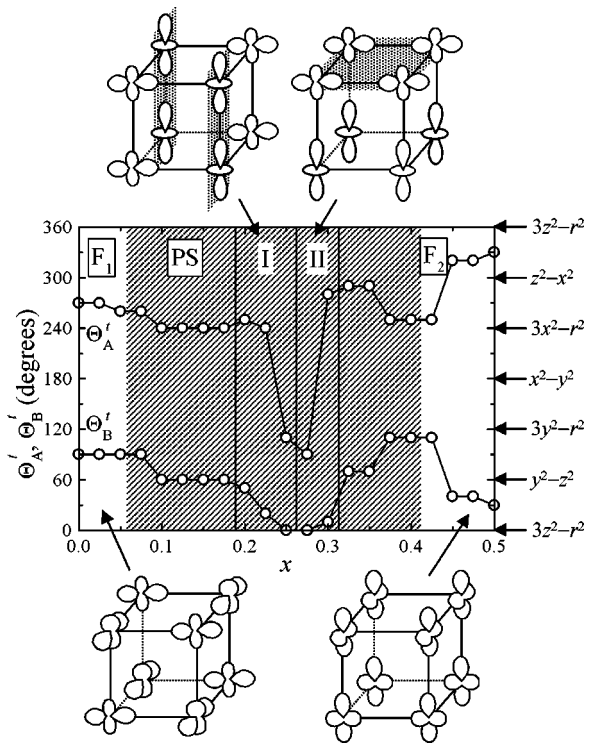

FIG. 4. A sequential change of orbital states as a function of hole concentration x. $\Theta^t_{A(B)}$ is the angle in the orbital space in the $A(B)$ orbital sublattice. The schematic orbital states are shown. In the phase-I and -II, the dotted areas show the region where the hole concentration is rich.

In order to investigate the stability of the PS state appearing between the F_1 and F_2 phases, the ground state energy is decomposed into the contributions from the SE interaction ($\langle\mathcal{H}_J\rangle$) and the DE one ($\langle\mathcal{H}_t\rangle$) [see Fig. 1(b)]. We find that with increasing x, $\langle\mathcal{H}_J\rangle$ increases and $\langle\mathcal{H}_t\rangle$ decreases. Several kinks appear in the $\langle\mathcal{H}_J\rangle$-$x$ and $\langle\mathcal{H}_t\rangle$-$x$ curves, which imply the discontinuous change of the state with changing x. The PS(F_1/F_2) state shown in Fig. 2 corresponds to the region, where the two ferromagnetic interactions compete with each other and the discontinuous changes appear in the $\langle\mathcal{H}_{J(t)}\rangle$-$x$ curve. In Fig. 4, we present the x dependence of the orbital state where PS state is not taken into account. The discontinuous change of $\langle\mathcal{H}_{J(t)}\rangle$-$x$ curve is ascribed to that of the orbital state. In particular, in phases I and II, the symmetry of the orbital is lower than that in the F_1 and F_2 phases and the stripe-type (quasi-one-dimensional) and sheet-type (two-dimensional) charge disproportion is realized, respectively. These remarkable features originate from the anisotropy in the orbital pseudospin space. We also note that because of the anisotropy, the orbital state dose not change continuously from F_1 to F_2. It is summarized that the main origin of the PS state in the ferromagnetic state is (1) the existence of two kinds of ferromagnetic interaction which favor the different types of orbital state and (2) the discontinuous change of orbital state due to the anisotropy in the orbital space unlike the spin case.

B. Phase diagram at finite T

In this subsection, we show the numerical results at finite T and discuss how the PS state changes with T. As the order parameter of spin, we assume the ferromagnetic ordering and focus on the F_1 and F_2 phases and the PS state between them. We consider the G- and F-type orbital orderings which are enough to discuss the orbital state in the ferromagnetic state of the present interest.

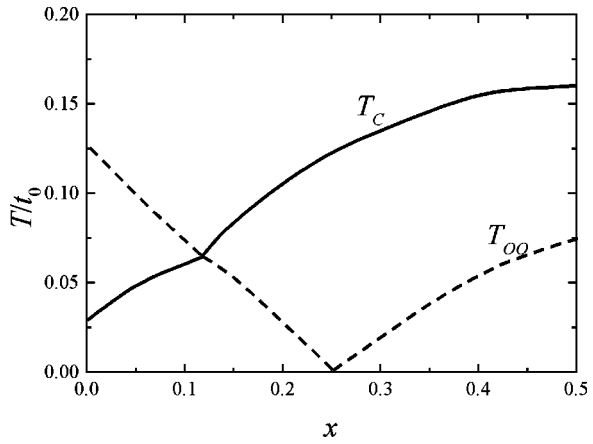

FIG. 5. The phase diagram in the plane of temperature (T) and hole concentration (x). The homogeneous state is assumed. The straight and dotted lines show the ferromagnetic Curie temperature (T_C) and the orbital ordered temperature (T_{OO}), respectively. The parameter values are chosen to be $J_1/t_0=0.25$, $J_2/t_0=0.0625$, and $J_{\mathrm{AF}}/t_0=0.004$.

In Fig. 5, the phase diagram is presented at finite T where the homogeneous phase is assumed. Parameter values are chosen to be $J_{\mathrm{AF}}/t_0=0.004$, $J_1/t_0=0.25$, and $J_2/t_0=0.0625$. At $x=0.0$, the orbital ordered temperature (T_{OO}) is higher than the ferromagnetic Curie temperature (T_C), because the interaction between orbitals ($3J_1/2$) in the paramagnetic state is larger than that between spins ($J_1/2$) in the orbital disordered state, as seen in the first term in $\mathcal{H}_J$. With increasing x, T_C monotonically increases. On the other hand, T_{OO} decreases and becomes its minimum around $x\sim0.25$. This is the consequence of the change of orbital ordering from G type to F type. The G- and F-type orbital orderings are favorable to the SE and DE interactions, respectively, so that the orderings occur in the lower and higher x regions. In Fig. 6(a), we present the free energy as a function of x at several temperatures. For $T/t_0<0.025$, the double minima around $x=0.1$ and 0.4 exist as discussed in the previous subsection at $T=0$. With increasing T, the double minima are gradually smeared out and a new local minimum appears around $x=0.3$. It implies that another phase becomes stable around $x=0.3$ and two different kinds of the PS state appear at the temperature. With further increasing temperature, several shallow minima appear in the $\mathcal{F}$-x curve. Finally, the fine structure disappears and the homogeneous phase becomes stable in the whole region of x. In Fig. 6(b), the free energy is decomposed into the contributions from $T\mathcal{S}$, $\langle\mathcal{H}_t\rangle$, and $\langle\mathcal{H}_J\rangle$ at $T/t_0=0.04$.

By applying the Maxwell construction to the free energy presented in Fig. 6(a), the PS states are obtained and presented in Fig. 7. The PS states dominate the large area in the x-T plane. A variety of the PS states appears with several types of spin and orbital states. Each PS state is represented by the combination of spin and orbital states, such as PS(spin-P, orbital-G/spin-F, orbital-P) for PS-III and

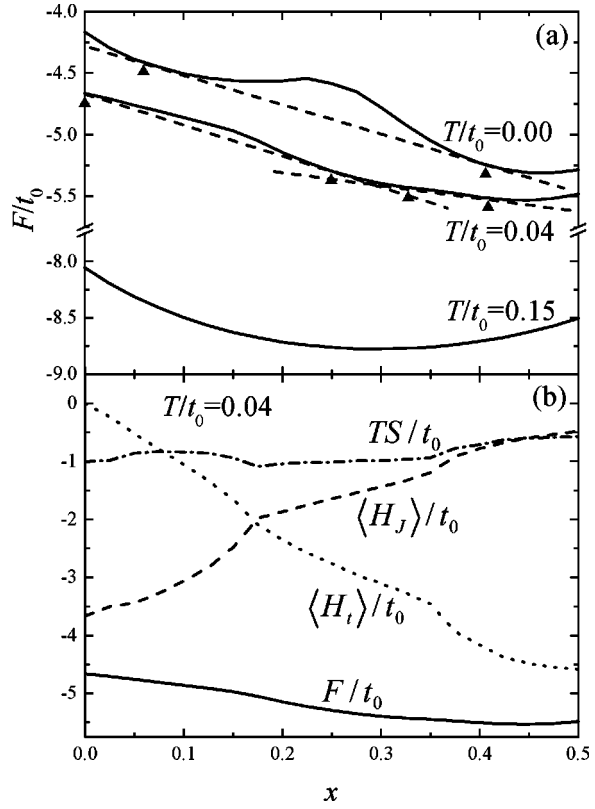

FIG. 6. The free energy as a function of hole concentration (x). (a): T/t_0 is chosen to be 0, 0.04, and 0.15. The broken lines and the filled triangles show the tangent lines of the $\mathcal{F}$-x curve and the points of contact between the two, respectively. (b): $\mathcal{F}$ is decomposed into the contributions from $T\mathcal{S}$, $\langle\mathcal{H}_t\rangle$, and $\langle\mathcal{H}_J\rangle$. T/t_0 is chosen to be 0.04.

PS(spin-F, orbital-G/spin-F, orbital-F)=PS(F_1/F_2) for PS-VII. Here, P indicates the paramagnetic (orbital) state. It is mentioned that the phase diagram in Fig. 7 has much analogy with that in eutectic alloys. For example, let us focus on the region below $T/t_0=0.05$. Here, the F_1 and F_2 phases and PS-VII correspond to the two kinds of homogeneous solid phases, termed A and B, and the PS state between them [PS(A/B)] in binary alloys, respectively. In the case of the binary alloys, the liquid(L) phase becomes stable due to the entropy at high temperatures. Thus, with increasing temperature, the successive transition occurs as PS(A/B) $\rightarrow$PS($L/A(B)$)$\rightarrow L$. The states L, PS(L/A), and PS(L/B), correspond to the (spin-F, orbital-P) phase, PS-V, and PS-VI in Fig. 7, respectively. By the analogy between two systems, the point at $T/t_0=0.025$ and $x=0.27$ corresponds to the eutectic point. In the $\mathcal{F}$-x curve shown in Fig. 6, above three states reflect on the three minima observed at $T/t_0=0.004$. By decomposing the free energy into the three terms $\langle\mathcal{H}_J\rangle$, $\langle\mathcal{H}_t\rangle$, and $T\mathcal{S}$, we confirm that the middle part corresponding to the (spin-F, orbital-P) phase is stabilized by the entropy.

In Fig. 8, we present effects of the magnetic field (B) on the phase diagram. The magnitude of the applied magnetic field is chosen to be $g\mu_B B/t_0=0.02$ which corresponds to 50 T for $t_0=0.3$ eV and $g=2$. We find that the PS state shrinks in the magnetic field. The remarkable change is observed in PS-II and -III where the spin-F and -P phases

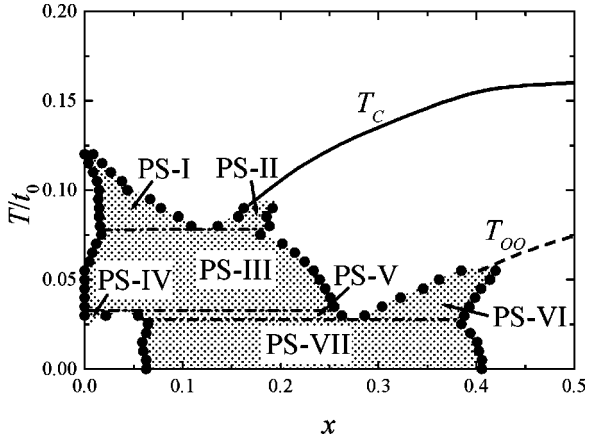

FIG. 7. The phase diagram at finite temperatures. The shaded area shows the phase separated region. The spin and orbital states in each state are PS-I: PS(spin-P,orbital-G/spin-P,orbital-P), PS-II: PS(spin-P,orbital-P/spin-F,orbital-P), PS-III: PS(spin-P,orbital-G/spin-F,orbital-P), PS-IV: PS(spin-P,orbital-G/spin-F,orbital-G), PS-V: PS(spin-F,orbital-G/spin-F,orbital-P), PS-VI: PS(spin-F,orbital-P/spin-F,orbital-F), and PS-VII: PS(spin-F,orbital-G/spin-F,orbital-F)=(F_1/F_2). The parameter values are the same as those in Fig. 5.

coexist. The magnetic field stabilizes the ferromagnetic phase so that the PS states are replaced by PS-V and the uniform ferromagnetic state. The region of PS-VII [PS(F_1/F_2)] is also suppressed in the magnetic field. Because the magnitude of the magnetization in the phase F_1 is smaller than that in the F_2 phase, the magnetic field stabilizes the F_1 phase.

V. SUMMARY AND DISCUSSION

In this paper, we study the spin and orbital phase diagram for perovskite manganites at finite T and x. In particular, we pay our attention to two kinds of ferromagnetic phase appearing at different hole concentrations. The SE and DE interactions dominate the ferromagnetic phases in the lightly and moderately doped regions and favor the AF- and F-type orbital orderings, respectively. Between the phases, the two

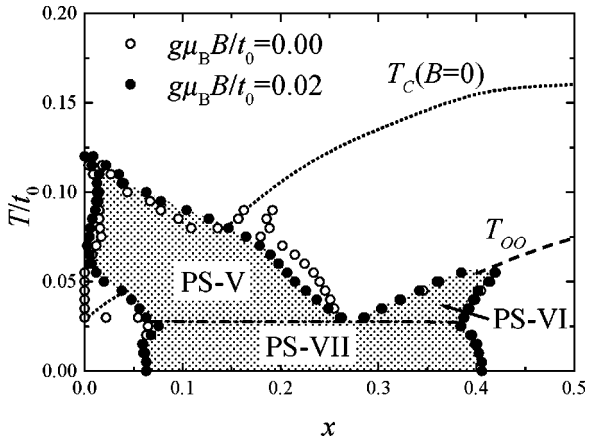

FIG. 8. The phase diagram at finite temperatures in the applied magnetic field (B). The open and filled circles show the boundary of the phase separated region in $g\mu_B B/t_0=0$ and 0.02, respectively. The other parameter values are the same as those in Fig. 5.

interactions compete with each other and the phases are unstable against the phase separation. The PS states at finite T have an analogy with that in the binary alloys.

It is worth making a comparison between the two kinds of PS, that is, the PS state between the two ferromagnetic phases with different orbital structures and that between the ferromagnetic and antiferromagnetic ones. Let us consider the case with $J_{\rm AF}/t_0=0.004$ in Fig. 2. We find PS(F_1/F_2) in the region with large x in comparison with PS(A-AF/F_1). This originates from the sequential change of the states with doping of holes as follows, I: (spin-A, orbital-G) $\rightarrow$ II: (spin-F, orbital-G) $\rightarrow$ III: (spin-F, orbital-F) where the PS state is not taken into account. The orbital state changes in the region with large x compared with the spin state, since the AF interaction between spins is much weaker than the AF-type one between orbitals at $x=0$. Thus, PS(A-AF/F_1) and PS(F_1/F_2) appear in the regions between I and II, and between II and III, respectively. We also note in Fig. 2 that PS(F_1/F_2) dominates a larger region in the phase diagram than PS(A-AF/F_1). This mainly results from the anisotropy in the orbital pseudospin space. As shown in Fig. 4, the angle in the orbital space $\Theta^t_{A(B)}$ changes discontinuously with x in the region of $0.06<x<0.41$ due to the anisotropy. This is highly in contrast to the spin case where the incommensurate and/or flux states appear in the intermediate doping region and some of them become more stable than the PS states.[23] It is mentioned furthermore that the PS state between the spin-F and spin-AF phases[24] discussed in the conventional double exchange model[25] is suppressed, when the orbital degree of freedom is taken into account. This is because the A-AF phase is realized at $x=0$ instead of the G-AF one and the ratio of the band width between the A-AF and F phases is $W_{\rm AF}/W_F=2/3$. This ratio is much larger than that between the G-AF and F phases which is of the order of $O(t_0/J_H)$. Therefore, the PS region, where the compressibility [$\kappa=(\partial\mu/\partial x)^{-1}$] is negative, shrinks. The ($d_{3x^2-r^2}/d_{3y^2-r^2}$)-type orbital ordering expected in undoped and lightly doped compounds further suppresses the PS state between spin-AF and spin-F, because the transfer intensity along the c axis is reduced and $W_{\rm AF}/W_F$ in this ordering is increased much more.

For observation of the PS(F_1/F_2) state proposed in this paper, the most direct probe is the resonant x-ray scattering which has recently been developed as a technique to observe the orbital ordering.[26,27] Here, the detailed measurement at several orbital reflection points are required to confirm the PS state where different orbital orderings coexist. The inhomogeneous lattice distortion may be observed in PS(F_1/F_2), although this is indirect. Several experimental results have reported an inhomogeneity in the lattice degree of freedom. Two kinds of Mn-O bond with different lengths are observed in $La_{1-x}Sr_xMnO_3$ by the pair distribution function analyses.[28] These values are almost independent of x, although the averaged orthohombicity decreases with x. In the compounds with ferromagnetic transition, full magnetic moment is observed at low temperatures. This fact excludes the coexistence of AF state and supports PS with different orbital orderings. The more direct evidence of PS was reported by the synchrotron x-ray diffraction in $La_{0.88}Sr_{0.12}MnO_3$.[29] Below 350 K, some of the Bragg peaks split and the minor phase with 20% volume fraction appears. This phase shows a larger orthohombic distortion than the major one. Thus, the experimental data are consistent with the existence of the PS state with different orbital structures. It is desired to carry out further investigations to clarify relations between the PS state proposed in this paper and the experimentally observed inhomogeneity in the lattice degree of freedom.

ACKNOWLEDGMENTS

The authors would like to thank Y. Endoh, K. Hirota, and H. Nojiri for their valuable discussions. This work was supported by the Grant in Aid from Ministry of Education, Science and Culture of Japan, CREST, and NEDO. S.O. acknowledges the financial support of the JSPS. Part of the numerical calculation was performed in the HITACS-3800/380 supercomputing facilities in IMR, Tohoku University.

[1] K. Chahara, T. Ohono, M. Kasai, Y. Kanke, and Y. Kozono, Appl. Phys. Lett. **62**, 780 (1993).
[2] R. von Helmolt, J. Wecker, B. Holzapfel, L. Schultz, and K. Samwer, Phys. Rev. Lett. **71**, 2331 (1993).
[3] Y. Tokura, A. Urushibara, Y. Moritomo, T. Arima, A. Asamitsu, G. Kido, and N. Furukawa, J. Phys. Soc. Jpn. **63**, 3931 (1994).
[4] S. Jin, T.H. Tiefel, M. McCormack, R.A. Fastnacht, R. Ramesh, and L.H. Chen, Science **264**, 413 (1994).
[5] C. Zener, Phys. Rev. **82**, 403 (1951).
[6] P.W. Anderson and H. Hasegawa, Phys. Rev. **100**, 675 (1955).
[7] K. Kubo and N. Ohata, J. Phys. Soc. Jpn. **33**, 21 (1972).
[8] N. Furukawa, J. Phys. Soc. Jpn. **63**, 3214 (1994); **64**, 3164 (1995).
[9] A.J. Millis, P.B. Littlewood, and B.I. Shraiman, Phys. Rev. Lett. **74**, 5144 (1995).
[10] J.B. Goodenough, Phys. Rev. **100**, 564 (1955); in *Progress in Solid State Chemistry*, edited by H. Reiss (Pergamon, London, 1971), Vol. 5.
[11] J. Kanamori, J. Phys. Chem. Solids **10**, 87 (1959).
[12] K.I. Kugel and D.I. Khomskii, Zh. Eksp. Teor. Fiz., Pis'ma Red. **15**, 629 (1972) [JETP Lett. **15**, 446 (1972)].
[13] K. Hirota, N. Kaneko, A. Nishizawa, and Y. Endoh, J. Phys. Soc. Jpn. **65**, 3736 (1996).
[14] S. Ishihara, J. Inoue, and S. Maekawa, Physica C **263**, 130 (1996); Phys. Rev. B **55**, 8280 (1997).
[15] H. Kawano, R. Kajimoto, M. Kubota, and H. Yoshizawa, Phys. Rev. B **53**, R14 709 (1996).
[16] Y. Endoh, K. Hirota, S. Ishihara, S. Okamoto, Y. Murakami, A. Nishizawa, T. Fukuda, H. Kimura, H. Nojiri, K. Kaneko, and S. Maekawa, Phys. Rev. Lett. **82**, 4328 (1999); H. Nojiri, K. Kaneko, M. Motokawa, K. Hirota, Y. Endoh, and K. Takahashi, Phys. Rev. B **60**, 4142 (1999).
[17] R. Maezono, S. Ishihara, and N. Nagaosa, Phys. Rev. B **57**, R13 993 (1998); **58**, 11 583 (1998).
[18] S. Yunoki, A. Moreo, and E. Dagotto, Phys. Rev. Lett. **81**, 5612 (1998).
[19] P.G. de Gennes, Phys. Rev. **118**, 141 (1960).
[20] S. Ishihara, M. Yamanaka, and N. Nagaosa, Phys. Rev. B **56**, 686

(1997).
[21] M. van Veenendaal and A.J. Fedro, Phys. Rev. B **59**, 1285 (1999).
[22] The *G*-type orbital ordering is degenerate with the *C*-type ordering.
[23] M. Yamanaka, W. Koshibae, and S. Maekawa, Phys. Rev. Lett. **81**, 5604 (1998); W. Koshibae, M. Yamanaka, M. Oshikawa, and S. Maekawa, *ibid.* **82**, 2119 (1999); J. Inoue and S. Maekawa, *ibid.* **74**, 3407 (1995).
[24] E.L. Nagaev, Phys. Status Solidi B **186**, 9 (1994).
[25] S. Yunoki, J. Hu, A.L. Malvezzi, A. Moreo, N. Furukawa, and D.E. Dagotto, Phys. Rev. Lett. **80**, 845 (1998); D.P. Arovas and F. Guinea, Phys. Rev. B **58**, 9150 (1998); S.-Q. Shen and Z.D. Wang, *ibid.* **58**, R8877 (1998); H. Yi and J. Yu, *ibid.* **58**, 11 123 (1998); M.Y. Kagan, D.I. Khomskii, and M. Mostovoy, cond-mat/9804213 (unpublished).
[26] Y. Murakami, H. Kawada, H. Kawata, M. Tanaka, T. Arima, H. Moritomo, and Y. Tokura, Phys. Rev. Lett. **80**, 1932 (1998); Y. Murakami, J.P. Hill, D. Gibbs, M. Blume, I. Koyama, M. Tanaka, H. Kawata, T. Arima, T. Tokura, K. Hirota, and Y. Endoh, *ibid.* **81**, 582 (1998).
[27] S. Ishihara and S. Maekawa, Phys. Rev. Lett. **80**, 3799 (1998); Phys. Rev. B **58**, 13 442 (1998).
[28] D. Louca, T. Egami, E.L. Brosha, H. Röder, and A.R. Bishop, Phys. Rev. B **56**, R8475 (1997).
[29] D.E. Cox, T. Iglesias, G. Shirane, K. Hirota, and Y. Endoh (unpublished).